

# One-Electron Charge and Spin Singular Branch Lines of the 1D Hubbard Model

J. M. P. Carmelo<sup>1</sup>, K. Penc<sup>2</sup>, L. M. Martelo<sup>1,3</sup>, P. D. Sacramento<sup>4</sup>,

J. M. B. Lopes dos Santos<sup>5</sup>, R. Claessen<sup>6</sup>, M. Sing<sup>6</sup>, and U. Schwingenschlög<sup>6</sup>

<sup>1</sup> GCEP-Center of Physics, University of Minho, Campus Gualtar, P-4710-057 Braga, Portugal

<sup>2</sup> Research Institute for Solid State Physics and Optics, H-1525 Budapest, P.O.B. 49, Hungary

<sup>3</sup> Physics Department, Engineering Faculty of University of Porto, P-4200-465 Porto, Portugal

<sup>4</sup> Departamento de Física and CFIF, Instituto Superior Técnico, P-1049-001 Lisboa, Portugal

<sup>5</sup> CFP and Departamento de Física FC Universidade do Porto, P-4169-007 Porto, Portugal and

<sup>6</sup> Experimentalphysik II, Universität Augsburg, D-86135 Augsburg, Germany

(Dated: 23 July 2003)

The momentum and energy dependence of the line shape in the vicinity of the one-electron spectral-function charge and spin singular branch lines of the 1D Hubbard model is studied for all values of the electronic density and on-site repulsion  $U$ . To achieve this goal we use a method which relies on the direct evaluation of the matrix elements between the energy eigenstates. Our theoretical predictions agree quantitatively for the whole momentum and energy bandwidth with the peak dispersions observed by angle-resolved photoelectron spectroscopy in the quasi-1D organic conductor TTF-TCNQ.

PACS numbers: 71.20.-b, 71.10.Pm, 72.15.Nj, 71.27.+a

The finite-energy spectral dispersions recently observed in quasi-one-dimensional (1D) metals by angle-resolved photoelectron spectroscopy (ARPES) reveal significant discrepancies from the conventional band-structure description [1, 2]. The study of the microscopic mechanisms behind these unusual finite-energy spectral properties remains until now an interesting open problem. There is some evidence that the correlation effects described by the 1D Hubbard model might contain such finite-energy mechanisms [1, 2]. However, in spite of the model Bethe-ansatz solution, for finite values of the on-site repulsion  $U$  very little is known about its finite-energy spectral properties, in contrast to simpler models [3]. Unfortunately, bosonization [4] and conformal-field theory [5] do not apply at finite energy. For  $U \rightarrow \infty$  the method of Ref. [6] provides valuable qualitative information, yet a quantitative description of the finite-energy spectral properties of quasi-1D metals requires the solution of the problem for finite values of  $U$ . The method of Ref. [7] refers to features of the insulator phase. For  $U \approx 4t$ , where  $t$  is the transfer integral, there are numerical results for the one-electron spectral function [8] which, unfortunately, provide very little information about the microscopic mechanisms behind the finite-energy spectral properties. Recent preliminary results obtained by use of the finite-energy holon and spinon description introduced in Refs. [9, 10, 11, 12] predict separate one-electron charge and spin spectral branch lines [11]. For the electron-removal spectral function these lines show quantitative agreement with the peak dispersions observed by ARPES in the quasi-1D organic conductor TTF-TCNQ [1]. However, these preliminary studies provide no information about the momentum and energy dependence of the line shape in the vicinity of the charge and spin branch lines and do not describe the TTF dispersion. The main goal of this letter is the evaluation of

such a dependence for all values of  $U$  and electronic density. In order to solve this complex many-electron problem, we use a powerful method described in Sec. V-B of Ref. [11]. Solution of the problem involves the computation of matrix elements between energy eigenstates by use of a pseudofermion description, as described in Sec. VII-B of Ref. [12].

The 1D Hubbard model can be written as  $\hat{H} = -t \sum_{j,\sigma} [c_{j,\sigma}^\dagger c_{j+1,\sigma} + h.c.] + U \sum_j \hat{n}_{j,\uparrow} \hat{n}_{j,\downarrow}$  where  $c_{j,\sigma}^\dagger$  and  $c_{j,\sigma}$  are spin  $\sigma = \uparrow, \downarrow$  electron operators at site  $j = 1, \dots, N_a$  and  $\hat{n}_{j,\sigma} = c_{j,\sigma}^\dagger c_{j,\sigma}$ . We consider the metallic phase with electronic density  $n = N/N_a$  in the range  $0 < n < 1$  and zero magnetization where  $N$  is the electron number. The Fermi momentum is  $k_F = \pi n/2$  and the electronic charge reads  $-e$ . The one-electron spectral function  $B_l(k, \omega)$  such that  $l = -1$  (and  $l = +1$ ) for electron removal (and addition) reads,

$$B_{-1}(k, \omega) = \sum_{\sigma, \gamma} |\langle \gamma | c_{k,\sigma} | GS \rangle|^2 \delta(\omega + \Delta E_{\gamma}^{N-1})$$

$$B_{+1}(k, \omega) = \sum_{\sigma, \gamma'} |\langle \gamma' | c_{k,\sigma}^\dagger | GS \rangle|^2 \delta(\omega - \Delta E_{\gamma'}^{N+1}), (1)$$

where  $c_{k,\sigma}$  and  $c_{k,\sigma}^\dagger$  are electron operators of momentum  $k$  and  $|GS\rangle$  denotes the initial  $N$ -electron ground state. The  $\gamma$  and  $\gamma'$  summations run over the  $N-1$  and  $N+1$ -electron excited states, respectively, and  $\Delta E_{\gamma}^{N-1}$  and  $\Delta E_{\gamma'}^{N+1}$  are the corresponding excitation energies.

The studies of Ref. [11] found and characterized the dominant microscopic processes which generate more than 99% of the electronic weight of the functions (1). Fortunately, the line shape in the vicinity of the branch lines we consider below is fully controlled by such dominant processes. Those involve the  $-1/2$  Yang holons and the  $c$ ,  $s$ ,  $1$ , and  $c$ ,  $1$  pseudoparticles studied in Refs.

[9, 10, 11]. For simplicity, we denote the latter two objects by  $s$  and  $c1$  pseudoparticles, respectively. The  $c$  pseudoparticle carries charge  $-e$  and has no spin and the  $s$  pseudoparticle is a spin-zero two-spinon composite object and has no charge. The  $c1$  pseudoparticle is a  $\eta$ -spin-zero two-holon composite object, carries charge  $-2e$ , and has zero spin. The  $-1/2$  Yang holon has  $\eta$ -spin  $1/2$ ,  $\eta$ -spin projection  $-1/2$ , charge  $-2e$ , and zero spin. The  $c$ ,  $s$ , and  $c1$  pseudoparticles carry band momentum  $q$  and have energy bands  $\epsilon_c(q)$ ,  $\epsilon_s(q)$ , and  $\epsilon_{c1}(q) = E_u + \epsilon_{c1}^0(q)$  such that  $|q| \leq \pi$ ,  $|q| \leq k_F$ , and  $|q| \leq [\pi - 2k_F]$ , respectively. These bands are studied in Refs. [9, 10] and plotted in Figs. 6-9 of Ref. [10].  $E_u$  defines the lower-limit of the *upper-Hubbard band* (UHB) [11] and equals the energy required for creation of a  $-1/2$  Yang holon, which is a dispersion-less object. It is such that  $E_u = 4t \cos(\pi n/2)$  for  $U/t \rightarrow 0$ ,  $E_u = U + 4t \cos(\pi n)$  for  $U \gg t$ ,  $E_u = U + 4t$  for  $n \rightarrow 0$ , and as  $n \rightarrow 1$   $E_u$  approaches the value of the Mott-Hubbard gap [10]. In the ground state there are no  $-1/2$  Yang holons, the  $c1$  and  $s$  pseudoparticle bands are empty and filled, respectively, and the  $c$  pseudoparticles occupy  $0 \leq |q| \leq 2k_F$  (leaving  $2k_F < |q| \leq \pi$  empty).

The ground state and excited states of Eq. (1) can be expressed in terms of occupancy configurations of the above quantum objects. The first step of the evaluation of the spectral functions (1) involves the expression of the electronic operators in terms of these quantum objects by use of the electron - rotated-electron unitary transformation, as described in Ref. [11]. For electron removal, the above dominant processes involve creation of one hole both in  $\epsilon_c(q)$  and  $\epsilon_s(q)$ . For electron addition, these dominant processes lead to two structures: A *lower-Hubbard band* (LHB) generated by creation of one particle in  $\epsilon_c(q)$  and one hole in  $\epsilon_s(q)$ ; A UHB generated by creation of one hole both in  $\epsilon_c(q)$  and  $\epsilon_s(q)$  and either one particle in  $\epsilon_{c1}^0(q)$  or one  $-1/2$  Yang holon. The domains of the  $(k, \omega)$  plane whose spectral weight is generated by dominant processes are shown in Fig. 1, where electron removal, LHB addition, and UHB addition corresponds to  $\omega < 0$ ,  $0 < \omega < E_u$ , and  $\omega > E_u$ , respectively. The dominant processes also include pseudoparticle particle-hole processes which lead to spectral weight both inside and outside but in the close vicinity of the shaded domains of Fig. 1. The next step involves the transformation of the pseudoparticles with residual interactions onto non-interacting pseudofermions [12]. The pseudofermion momentum has a unusual functional term which is controlled by the phase shifts  $\Phi_{\alpha\alpha'}(q, q')$  defined in Ref. [12], where  $\alpha, \alpha' = c, s, c1$ . Since the pseudofermions are non-interacting, the spectral functions (1) can be expressed as a convolution of single pseudofermion spectral functions. The derivation of matrix elements between the ground state and excited states for pseudofermion operators proceeds as in Ref. [6] for the spin-less fermions [12]. One finds that both the singularities and spectral-weight

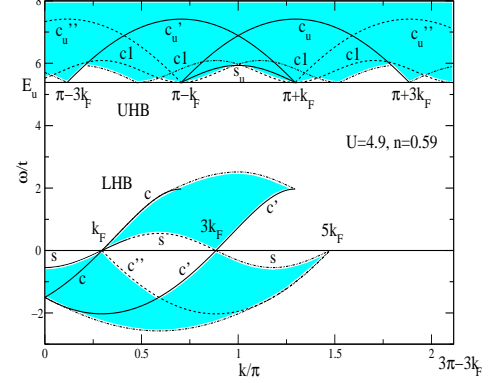


FIG. 1: Extended-zone scheme centered at  $k = 0$  (and at  $k = \pi$  for the UHB) for  $U = 4.9t$  and  $n = 0.59$ . The shaded areas weight is generated by dominant processes.

edges are located on pseudofermion branch lines. Such lines are generated by processes where a pseudofermion is created or annihilated for the available values of momentum  $q$  and the remaining quantum objects are created or annihilated at their *Fermi points*. The singular and edge branch lines are represented in Fig. 1 by solid and dashed lines, respectively. The edge branch lines are controlled by positive exponents smaller than one. Finally, the dashed-dotted lines are either border lines of the above domains or branch lines associated with exponents larger than one and have very little weight.

For simplicity, in this letter we consider the exponents that control the line shape in the vicinity of singular branch lines only. However, similar expressions can be evaluated for any branch line. The singular branch lines correspond to all the  $(k, \omega)$  regions where there are line-shape singularities. While it is difficult to measure the critical exponents experimentally, a crucial test for the suitability of the model to describe real quasi-1D materials is whether the ARPES peak dispersions correspond to the predicted singular branch lines. We start by considering the spin  $s$  branch line for  $0 < k < 3k_F$ , the charge  $c$  branch line for  $0 < k < \pi - k_F$ , and the charge  $c'$  branch line for  $0 < k < \pi + k_F$  (see Fig. 1). The parametric equations that define these branch lines read  $\omega(k) = \epsilon_s(q)$  for the  $s$  line where  $q = q(k) = (1+l)k_F - lk$  for  $(1+l)k_F/2 < k < k_F + (1+l)k_F$  and  $\omega(k) = \epsilon_\alpha(q)$  for the  $\alpha = c$  line ( $l' = +1$ ) and  $\alpha = c'$  line ( $l' = -1$ ) where  $q = q(k) = k + l'k_F$  for  $0 < k < \pi - l'k_F$ . Here,  $\epsilon_{c'}(q) \equiv \epsilon_c(q)$ . The following expressions describe the line shape in the vicinity of the  $\alpha = s, c, c'$  branch lines for  $\omega$  values such that  $(\epsilon_\alpha(q) + l\omega)$  is small and positive,

$$B_l(k, \omega) = C_\alpha^l(k) \left( \epsilon_\alpha(q) + l\omega \right)^{\zeta_\alpha(k)}; \quad \alpha = s, c, c'. \quad (2)$$

Here the expression of  $C_\alpha^l(k)$ , such that  $C_\alpha^l(k) > 0$  for  $U/t > 0$ , is very involved and will be studied numerically elsewhere. For  $U/t \rightarrow 0$  it behaves as  $C_s^l(k) \rightarrow \delta_{l,-1}$ ,  $C_c^l(k) \rightarrow \delta_{l,+1}$ , and  $C_{c'}^l(k) \rightarrow 0$ . The exponents read,

$$\begin{aligned}\zeta_s(k) &= -1 + \sum_{l=\pm 1} \left\{ \frac{1}{2\sqrt{2}} - l \Phi_{ss}(l k_F, q) \right\}^2 \\ &\quad + \sum_{l=\pm 1} \left\{ \frac{l}{2\xi_0} + \frac{(1+l)\xi_0}{4} - l \Phi_{cs}(l 2k_F, q) \right\}^2; \\ \zeta_\alpha(k) &= -1 + \sum_{l=\pm 1} \left\{ \frac{1-l(1+l'l')}{2\sqrt{2}} + l \Phi_{sc}(l k_F, q) \right\}^2 \\ &\quad + \sum_{l=\pm 1} \left\{ \frac{1-l(1-\xi_0)}{4} - l' \Phi_{cc}(l 2k_F, q) \right\}^2, \quad (3)\end{aligned}$$

where  $\alpha = c$  for  $l' = +1$  and  $\alpha = c'$  for  $l' = -1$ . In the exponent expressions the phase shifts are defined in Ref. [12] and  $\xi_0 \equiv \sqrt{2K_\rho}$  where  $K_\rho$ , such that  $K_\rho \rightarrow 1$  as  $U/t \rightarrow 0$  and  $K_\rho \rightarrow 1/2$  as  $U/t \rightarrow \infty$ , is defined in Ref. [4]. The exponents  $\zeta_s(k)$  and  $\zeta_{\alpha=c,c'}(k)$  are plotted in Figs. 2 and 3, respectively, as a function of  $k$  for several values of  $U/t$  and  $n = 0.59$ . The exponent  $\zeta_c(k)$  (and  $\zeta_{c'}(k)$ ) is plotted in Fig. 3 (a) and (b) (and Fig. 3 (c) and (d)) for  $l = -1$  and  $l = +1$ , respectively. As  $U/t \rightarrow \infty$  these exponents behave as  $\zeta_s(k) = -1/2 + 2(q/4k_F)^2$  and  $\zeta_s(k) = -(q/2k_F)[1 - (q/4k_F)]$  for  $l = -1$  and  $l = +1$ , respectively, and  $\zeta_c(q) = \zeta_{c'}(q) = -3/8$ , in agreement with Ref. [6]. The line shape of the UHB singular branch lines of Fig. 1 is controlled by the same exponents as the corresponding electron-removal branch lines studied above. For  $0 < k < \pi$  the parametric equations of the  $s_u$  branch line for  $\pi - k_F < k < \pi$ ,  $c_u$  branch line for  $\pi - k_F < k < \pi$ , and  $c'_u$  branch line for  $\pi - 3k_F < k < \pi$  is the same as for the corresponding  $s$ ,  $c$ , and  $c'$  branch lines, respectively, provided that  $k$  is replaced by  $\pi - k$  and  $\omega$  by  $E_u - \omega$  in the parametric equations of the latter lines. Under such a replacement the critical exponents that control the line shape of these UHB lines are the same as for the corresponding electron-removal lines. While in the limit  $n \rightarrow 1$  such a correspondence refers also to the value of the constant  $C_{\alpha}^{-1}(k)$  of Eq. (2), otherwise the corresponding UHB constant  $C_{\alpha u}^{+1}(\pi - k)$  is slightly smaller. This is because for  $n < 1$  there is also weight in the vicinity of the four  $c1$  pseudofermion branch lines of Fig. 1. We omit here the study of the line shape of these lines whose critical exponents are positive.

When the exponents (3) tend to  $-1$  as  $U/t \rightarrow 0$  the expression (2) is replaced by  $\delta(\epsilon_\alpha(q) + l\omega)$ . For  $0 < k < \pi$  and  $U/t \rightarrow 0$  all spectral weight is transferred over to the  $s$  branch line for  $0 < k < k_F$ ,  $c$  branch line for  $k_F < k < \pi - k_F$ , and  $s_u$  branch line for  $\pi - k_F < k < \pi$ . There is no weight in other branch lines and  $k > 0$  regions of the  $(k, \omega)$  plane in such a limit. The two points  $(k = \pi - k_F, \omega = E_u)$  and  $(k = \pi - k_F, \omega = \epsilon_c(\pi))$  where  $q = \pi$  corresponds to  $k = \pi - k_F$  become the same point as

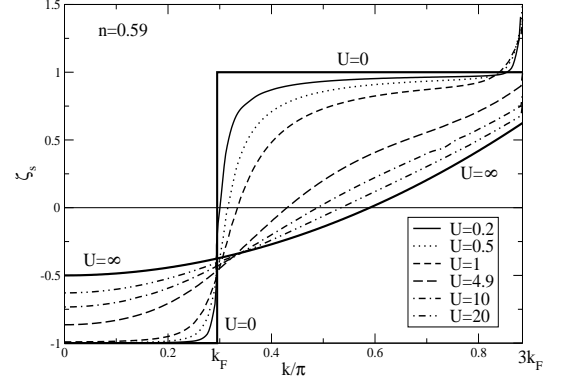


FIG. 2: Momentum dependence along the spin  $s$  branch line of the critical exponent (3).

$U/t \rightarrow 0$  and the  $c$  and  $s_u$  branch lines become connected at such a point (see Fig. 1 for  $U/t = 4.9$ ). By use of the  $U/t \rightarrow 0$  expressions (A1) and (A2) of Ref. [10] for  $\epsilon_c(q)$  and  $\epsilon_s(q)$ , one finds that these three branch lines give rise to the electronic spectrum  $\omega(k) = -2t[\cos(k) - \cos(k_F)]$ . Consistently, the above corresponding exponents are such that  $\zeta_s(k) \rightarrow -1$  for  $0 < k < k_F$ ,  $\zeta_c(k) \rightarrow -1$  for  $k_F < k < \pi - k_F$ , and  $\zeta_{s_u}(k) = \zeta_s(\pi - k) \rightarrow -1$  for  $\pi - k_F < k < \pi$  as  $U/t \rightarrow 0$ . Then the correct non-interacting electronic spectral function is reached as  $U/t \rightarrow 0$ . (For  $U/t \rightarrow 0$  the exponents (3) behave as  $\zeta_s(k) = l = \pm 1$ ,  $\zeta_\alpha(q) = -1/\sqrt{2} + 1/2$  for  $\alpha = c, c'$  and  $l = -1$ , and  $\zeta_c(q) = -1$  and  $\zeta_{c'}(q) = 1$  for  $l = +1$ .)

An interesting realization of a 1D metal is the organic charge-transfer salt TTF-TCNQ [2]. The experimental dispersions in the electron removal spectrum of this quasi-1D conductor as measured by ARPES are shown in Fig. 4. The data were taken with He I radiation (21.2 eV) at a sample temperature of 60 K on a clean surface obtained by *in situ* cleavage of a single crystal. Instrumental energy and momentum resolution amount to 70 meV and  $0.07 \text{ \AA}^{-1}$ , respectively. The experimental data in Fig. 4 reproduce earlier work [1, 2]. While our above theoretical line-shape expressions refer to all values of  $U/t$  and  $n$ , we find that the electron removal spectra calculated for  $t = 0.4 \text{ eV}$ ,  $U = 1.96 \text{ eV}$  ( $U/t = 0.49$ ), and  $n = 0.59$  yields an almost perfect agreement with the three TCNQ experimental dispersions. If accounted for a renormalization of the transfer integral due to a possible surface relaxation [1], these values are in good agreement with estimates from other experiments [2]. We note that the low-energy behavior is not correctly reproduced due to the "pseudogap" behavior in the data [1]. The experimental TCNQ finite-energy peak dispersions of Fig. 4 correspond to the spin  $s$  branch line and charge  $c$  and  $c'$  branch lines. Importantly, only these singular branch lines, whose line shape is controlled by negative exponents, lead to peak dispersions in the real experiment. The other peak dispersion of Fig. 4 is as-

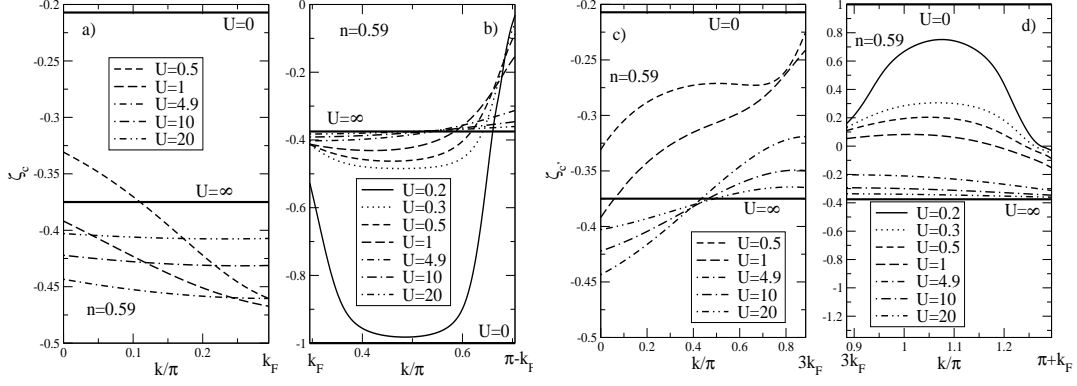


FIG. 3: Momentum dependence of the critical exponent (3) along (a) and (c) the electron-removal and (b) and (d) electron-addition charge  $c$  and  $c'$  branch lines, respectively.

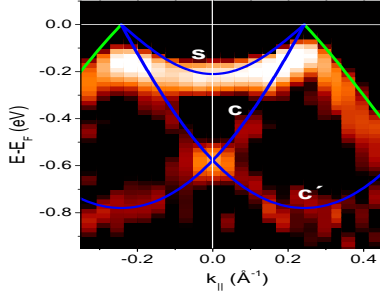


FIG. 4: Angle-resolved photoemission spectra of TTF-TCNQ measured along the easy transport axis and matching theoretical branch lines.

sociated with the electron-removal spectrum of the TTF chains whose density is  $n = 2 - 0.59 = 1.41$ . It can be described by the electron-addition spectrum of a corresponding  $n = 0.59$  problem. Remarkably, we find again that the theoretical lines match the TTF dispersion provided that  $t \approx 0.27$  eV and  $U < 0.2t$  within experimental uncertainty. Indeed, for such small values of  $U/t$  and  $n = 0.59$  both the electron-addition exponents of Figs. 2 and 3 (d) are positive, whereas the exponent of Fig. 3 (b) and the UHB exponent  $\zeta_{su}(k) = \zeta_s(\pi - k)$  for  $\pi - k < k_F$  (see Fig. 2) are negative. For  $n = 1.41$  the  $c$  and  $s_u$  lines associated with these exponents correspond to electron removal and thus appear at negative values of  $\omega$  and lead to a single singular branch line formed by the  $c$  line for  $0.59\pi/2 < k < 1.41\pi/2$  and the  $s_u$  line for  $1.41\pi/2 < k < \pi$ . The energy pseudogap at  $k = 1.41\pi/2$ , which separates the  $c$  line from the  $s_u$  line, nearly vanishes for  $U/t < 0.2t$  and thus is not observed in the experiment. This singular branch line is

that matching the TTF peak dispersion of Fig. 4. (It matches such a dispersion for  $0.59\pi/2 < k < \pi$ .) We thus conclude that in contrast to the conventional band structure description, the singular branch lines obtained from the 1D Hubbard model describe quantitatively, for the whole finite-energy band width, the peak dispersions observed by ARPES in TTF-TCNQ. This seems to indicate that the dominant non-perturbative many-electron microscopic processes found and studied in Refs. [11, 12], which control the line shape of these charge and spin singular branch lines, also control the unusual finite-energy spectral properties of TTF-TCNQ.

K.P. thanks the financial support of OTKA grants D032689 and T037451, L.M.M. of FCT grant BD/3797/94, and R.C., M.S., and U.S. of Deutsche Forschungsgemeinschaft (CL 124/3-3 and SFB 484).

- 
- [1] M. Sing *et al.*, cond-mat/0304283.
  - [2] R. Claessen *et al.*, Phys. Rev. Lett. **88**, 096402 (2002); F. Zwick *et al.*, *ibid.* **81**, 2974 (1998); S. Kagoshima, H. Nagasawa, and T. Sambongi, *one-dimensional conductors* (Springer, Berlin, 1987), and references therein.
  - [3] M. Arikawa, Y. Saiga, and Y. Kuramoto, Phys. Rev. Lett. **86**, 3096 (2001); Karlo Penc and B. Sriram Shastry, Phys. Rev. B **65**, 155110 (2002).
  - [4] H. J. Schulz, Phys. Rev. Lett. **64**, 2831 (1990).
  - [5] Holger Frahm and V. E. Korepin, Phys. Rev. B **42**, 10 553 (1990).
  - [6] Karlo Penc, Karen Hallberg, Frédéric Mila, and Hiroyuki Shiba, Phys. Rev. Lett. **77**, 1390 (1996); *ibid.* Phys. Rev. B **55**, 15 475 (1997).
  - [7] S. Sorella and A. Parola, Phys. Rev. Lett. **76**, 4604 (1996).
  - [8] D. Sénéchal, D. Perez, and M. Pioro-Ladrière, Phys. Rev. Lett. **84**, 522 (2000).
  - [9] J. M. P. Carmelo, K. Penc, and J. M. Román, cond-mat/0302044; J. M. P. Carmelo, cond-mat/0305347.
  - [10] J. M. P. Carmelo and P. D. Sacramento, Phys. Rev. B **68** (2003) [cond-mat/0302042].
  - [11] J. M. P. Carmelo and K. Penc, cond-mat/0303279.

- [12] J. M. P. Carmelo, cond-mat/0305568.